Ab initio Hartree-Fock investigation of the structural, electronic, and magnetic properties of Mn_3O_4

Alain Chartier and Philippe D'Arco
Laboratoire de Pétrologie, Case 110, UPMC Tour 26, 4, place Jussieu, 75252 Paris Cedex 05, France

Roberto Dovesi
Dipartimento di Chimica Inorganica, Chimica Fisica e Chimica dei Materiali, Università di Torino, via Pietro Giuria 5, I-10125 Torino, Italy

Victor R. Saunders
CLRC Daresbury Laboratory, Warrington WA4 4AD, United Kingdom
(Received 6 April 1999)

Noncubic Mn_3O_4 spinel (Hausmannite) has been investigated by using the periodic Hartree-Fock CRYSTAL95 program. The structure has been fully optimized, and the computed geometry compares well with the experimental data. The analysis of the wave function in terms of Mulliken charges shows that the net charge of the tetrahedral cation (Mn_A) is very close to the formal one ($+1.86$ electrons to be compared to $+2$); for the octahedral site (Mn_B) the net charge is far from the ideal ionic model ($+2.3$ electrons instead of $+3$), and the Mn_B-O bonds show some covalent character. The same analysis performed on the spin density gives magnetic moments very close to the ones corresponding to the ideal d^4 and d^5 configurations (4.90 and 3.97 electrons for Mn_A and Mn_B, respectively). The total energy of seven different spin configurations has been evaluated and the corresponding wave function analyzed. Superexchange coupling constants are evaluated by mapping the *ab initio* energy data to the Ising hamiltonian. It turns out that the intertetrahedral and tetrahedral-octahedral magnetic interactions are small and antiferromagnetic, in agreement with experimental evidence. The Mn_B-Mn_B along the octahedra chains is ten times larger, whereas the interchain interaction is small and ferromagnetic. [S0163-1829(99)03843-6]

I. INTRODUCTION

Substantial progress towards a full *ab initio* account of the structural and electronic properties of important classes of crystalline compounds such as simple metals, semiconductors, ceramics and silicates has been achieved in recent years. For other classes of compounds, such as transition metal (TM) ionics (oxides, sulfides, halides), *ab initio* methods have been less successful. Simple properties such as the insulating character of these materials and the relative stability of their ferro- and antiferromagnetic states remained out of reach for a long period. The situation has, however, changed when the Unrestricted Hartree-Fock option has been implemented in the CRYSTAL95 code.[1] Since then, the electronic and magnetic properties of many (about 30) TM oxides and halides (including MO oxides,[2–4] M_2O_3 sesquioxides,[5–8] KMF_3 perovskites and K_2MF_4 layered perovskites,[9–12] MF_2 rutiles,[13,14] where M is one or more of the first row transition metals) have been successfully investigated. The three-, two-, or one-dimensional antiferromagnetic character of the magnetic interaction in these compounds is correctly reproduced; the magnitude of the superexchange coupling constants (evaluated by mapping the *ab initio* data to model Hamiltonians), its dependence on the M-M distance and M-X-M angle (X is the anion) are in good agreement with experimental evidence.[15]

The high quality of the results obtained in the description of these simple materials encouraged us to tackle the more difficult task represented by Mn_3O_4. Mn_3O_4 hausmannite is to be considered as a *difficult* system from the point of view of the *ab initio* simulation for many reasons:

1. It has a tetragonally distorted spinel structure, with a relatively low symmetry and 14 atoms in the unit cell.
2. It contains six transition metal atoms.
3. Two Mn atoms are expected to have an electronic configuration close to d^5, four to d^4.
4. The latter is expected to give rise to a Jahn-Teller distortion.

All these features represent on the one hand challenging tests for the *ab initio* simulation, and make on the other hand this system extremely interesting.

Much attention has been devoted to its magnetic properties,[16–19] and to its canted spin structure. It is a good prototype of the spinel compounds displaying Jahn-Teller distortion; the effect of the substitution of other transition metals, such as Cr, on its structural and magnetic properties has been extensively analyzed.[20] Its behavior as a function of temperature and pressure[21] has been investigated too. At room pressure and temperature it is tetragonal; at high temperature (1160 °C) it becomes cubic. At high pressure (10 GPa) and temperature (900 °C), it converts to an orthorhombic phase isostructural to marokite $CaMn_2O_4$.[22]

The paper is organized as follow. The structure of Mn_3O_4 is illustrated in Sec. II. Section III is devoted to the computational method. The results, presented in Sec. IV, are organized in three subsections devoted to the structural data, the electronic structure and the magnetic properties. In Sec. V, some conclusions are drawn.

TABLE I. Experimental and calculated structural data. a and c are the lattice parameters (in Å), y and z are the fractionary coordinates of oxygen. A, B, a, and e label the tetrahedral and octahedral cations and the apical and equatorial Mn-O distances, respectively. α_A and β_A are the two tetrahedral angles. α_B and β_B are the largest O_a-Mn-O_e and O_e-Mn-O_e angles, respectively. The data in the first two lines refer to the present calculation without (nd) and with (d) d orbitals on oxygen. Other labels refer to experimental determinations.

a	c	y	z	Mn_A-O	Mn_B-O_a	Mn_B-O_e	α_A	β_A	α_B	β_B	ref
5.919	9.311	0.2157	0.3846	2.098	2.247	1.956	106.65	110.90	96.54	98.53	nd
5.882	9.481	0.2166	0.3846	2.099	2.287	1.947	105.12	111.68	96.39	98.29	d
5.76	9.46	0.216	0.384	2.069	2.288	1.905	104.47	112.03	96.27	98.44	25
5.765	9.442	0.2222	0.3839	2.040	2.282	1.930	103.42	112.58	95.50	96.84	26
5.756	9.439	0.227	0.383	2.011	2.288	1.945	102.75	112.93	94.68	95.60	17
5.71	9.35	0.2208	0.3834	2.028	2.259	1.906	103.94	112.31	95.52	97.18	18

II. SKETCH OF THE STRUCTURE

At low temperature and room pressure, Mn_3O_4 has a tetragonally distorted spinel structure (space group $I4_1/amd$), with two formula units per primitive cell. There are two different kinds of manganese atoms in the cell: Mn_A, sitting at (0,0,0), which is a 4-a tetrahedral site and Mn_B, located at (0,1/4,5/8) in a 8-d octahedral site. All the oxygen atoms are equivalent, and are at $(0,y,z)$, which is a 16-h position. Experimental values for the four cell parameters (a,c,y,z) are given in Table I. The MnO_4 tetrahedron is angularly distorted: there are two kinds of O-Mn_A-O angles (103.4 and 112.6 degrees); the four Mn_A-O distances are equivalent, and equal to 2.040 Å. The octahedron too is distorted, with two apical distances equal to 2.282 Å and four equatorial distances equal to 1.930 Å (see Fig. 1). All the O-Mn_B-O angles deviate from 90° by about 5°. Each oxygen is fourfold coordinated (to three Mn_B and one Mn_A, see Fig. 1). In terms of polyhedral representation of the structure, each octahedron shares edges with six different surrounding octahedra. The structure can then be described as formed by chains of octahedra running parallel to the $\underline{a}$ and $\underline{b}$ lattice vectors (Fig. 2). The $\underline{a}$ and $\underline{b}$ chains are orthogonal, and connected by shared edges. First nearest Mn_B-Mn_B neighbors occur along the $\underline{a}$ (or $\underline{b}$) chain (B-3-B path in Fig. 1); their distance is equal to 2.96 Å (the two Mn_B-O bonds are equatorial, and the Mn_B-O-Mn_B angle is 98.3°). Second nearest Mn_B-Mn_B neighbors belong to orthogonal chains; their distance is equal to 3.13 Å (B-3-B' path in Fig. 1, one apical and one equatorial bond with a Mn_B-O-Mn_B angle equal to 96.0°). First and second Mn_B-Mn_A neighbors are at 3.51 and 3.79 Å (B-3-A and B'-3-A in Fig. 1, where one equatorial and one apical octahedral bond are involved, respectively; the angles are equal to 119.7, 121.5 degrees, respectively).

III. COMPUTATIONAL DETAILS

For the present calculations, the CRYSTAL95 program has been adopted, in its Unrestricted Hartree-Fock (UHF) version, that permits us to investigate spin polarized systems. CRYSTAL95 is a periodic *ab initio* code that uses a variational basis set of localized functions, and can solve both the Hartree-Fock and Kohn-Sham equations. We refer to previous papers[1,23] for a description of the main features of the method and code. Tools have been implemented in CRYSTAL95 in order to address the system towards the required spin solution (seven in the present case). It is, how-

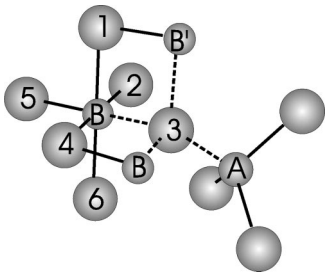

FIG. 1. Local coordination of oxygen and A (tetrahedral) and B (octahedral) manganese atoms. Atoms 2, 3, 4, and 5 lie in the equatorial plane (short Mn-O distance); oxygens 1 and 6 are apical (long distance). Oxygen 3 is fourfold coordinated through two short (B) and one long (B') octahedral bonds, and one (A) tetrahedral bond. Four superexchange paths are represented in the figure: B-3-B,B-3-B',B-3-A,B'-3-A. The corresponding superexchange coupling constants will be indicated as J_{BBs}, J_{BBl}, J_{AB} and $J_{AB'}$. Two A sites are not directly connected (the path could be A-3-B-4-A); nevertheless the corresponding J_{AA} coupling constant is not negligible.

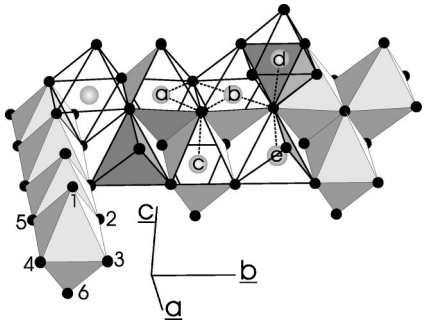

FIG. 2. Polyhedral representation of the hausmannite structure. Octahedral chains are parallel to the $\underline{a}$ and $\underline{b}$ lattice vectors. Two tetrahedra are also represented; they are linked to the same octahedron (with atom c at the center) through a corner. Black dots represent oxygen atoms; labels 2,3,4,5 and 1,2,6,4 define the equatorial and vertical planes of the charge density maps (see text). The a, b, c, d letters label manganese atoms at the center of octahedra; e is at a tetrahedral site. Dotted lines indicate superexchange paths connecting two manganese atoms via an oxygen atom.

ever, to be underlined that only the total number of unpaired electrons in the unit cell is imposed *a priori*, whereas the partition of the spin density between the transition metal atoms (four Mn_B and two Mn_A in the present case) is not constrained. The final spin configuration in the unit cell is then the result of a variational calculation with the constraint of an *a priori* defined number of α-β electrons for each explored spin state.

As regards the computational conditions, the numerical tolerances used in the evaluation of the infinite bielectronic Coulomb and exchange series were identical to those adopted in recent studies,[6,12,24] and chosen to ensure high numerical accuracy. The shrinking factor, IS, which defines the reciprocal space net, was set to 4, corresponding to 13 **k** points at which the Fock matrix is diagonalized. Larger shrinking factors do not yield significant change in energy.

As regards the basis set, Bloch functions are constructed from local function (''atomic orbitals''), which in turn are linear combinations (''contractions'') of Gaussian-type functions (GTF's), that are the product of a Gaussian and a real solid spherical harmonic. The all-electron basis sets used for the present study were previously used for MnO,[2,4] and contains 18 atomic orbitals for O and 27 atomic orbitals for Mn. This basis set can be denoted as a $8-411G^{\star}$ and 8-6-411-(41*d*)*G* contraction for O and Mn, respectively. The exponents (α) of the most diffuse single gaussian shells have been reoptimized by searching for the minimum crystal total energy. For oxygen, the best values are $\alpha(sp)=0.455$, $\alpha(sp)=0.175$, and $\alpha(d)=0.463$. For Mn, also the scale factor λ of the 4*G d* contraction has been optimized, and the optimization has been performed separately for Mn_A and Mn_B. The obtained values are $\lambda_A(d)=1.024$, $\alpha_A(d)=0.28$ and $\lambda_B(d)=1.018$, $\alpha_B(d)=0.28$. These values show that the basis sets for the two sites are very close, and close to the one optimized in MnO.

IV. RESULTS AND DISCUSSION

A. Structural data

The equation of state has been evaluated as follows: for eight cell volumes, the total energy of the system has been minimized with respect to the *c/a* ratio and *y* and *z* oxygen fractional coordinates, for the ferromagnetic state (FEM). The resulting energy versus volume curve has been fitted with a Murnaghan equation of state. The equilibrium volume (328.0 Å) is about 4% larger than the experimental one (314.8 ± 6.7 Å), in line with previous Hartree-Fock calculations (see for example[24]). The calculated geometry is compared with the experimental ones in Table I. The table reports also the geometry obtained with a poorer basis set, with no *d* functions on oxygen; this basis set has been used for the calculation of the many FIM (ferrimagnetic) structures, to be discussed in the magnetic section; these structures, for their low symmetry, are very demanding from a computational point of view, and could not be investigated with the richer basis set. The geometry calculated with the larger basis set reproduces fairly well experimental bonds (the tetrahedral and octahedral Mn-O bonds are overestimated by about 0.06 and 0.02 Å, respectively) and angles (the largest differences are of the order of 2°–3°). Also the *c/a* ratio is well reproduced (1.61 to be compared to 1.64[17,18,25,26]); these values can be compared to 1.414 (or $\sqrt{2}$), which is the *c/a* value corresponding to the ideal cubic structure when described within the tetragonal symmetry. The agreement is much poorer when *d* functions are not present on oxygen, as basis set is not flexible enough to allow for the polyhedra distortion. The calculated bulk modulus *B* is equal to 167 GPa, and its pressure-derivative B' equals 6.1. A recent low temperature measurent gives a value of 137 GPa with B' set to 4.[21] The overestimation of *B* (about 20%) is in line with previous calculations performed on other spinel compounds[27] with similar basis sets, and 5% to 10% larger than the one expected when a very rich basis set is used.[28]

The Hartree-Fock (HF) binding energy (BE), calculated as the difference between the bulk and the atomic energies, is 1692 kJ mol^{-1}, which represents about 52% of the experimental BE (3234 kJ mol^{-1}) obtained from the enthalpy of formation of Mn_3O_4[29] and atomization energies of Mn and O. An *a posteriori* correction, that takes into account the correlation contribution to BE, and is evaluated through a *correlation-only* functional applied to the HF charge density, improves dramatically the calculated BE (2615 kJ mol^{-1}, corresponding to 82% of the experimental value). This value is in line with the BE obtained for MnO[2] and other oxides.[30]

B. The electronic structure

The net charges of the three atoms, evaluated according to a Mulliken partition of the charge density, are +1.858 (Mn_A), +2.292 (Mn_B) and $-1.61|e|$ (oxygen), respectively. The system appears then quite ionic, although the charges are far from the formal ones corresponding to the ideal ionic situation (+2, +3, and $-2|e|$), in particular in the case of the octahedral Mn atom.

The spin population analysis provides, on the contrary, values much closer to the formal ones: 4.90 and $3.97|e|$ for Mn_A and Mn_B, respectively, to be compared to 5 and 4 corresponding to d^5 and d^4 high spin atomic configurations. Values derived from neutron scattering experiments range from 3.25 to 3.64[17,18] for Mn_A, and from 4.65 to 5.34 for Mn_B. Mn_A is then essentially in the same Mn^{2+} d^5 electronic configuration already observed for MnO.[2,4] For Mn_B a deeper analysis of the data given in Table II is required. A local frame is assumed, with the *z* axis along the apical Mn-O bond of the octahedron, and the *x* axis along one of the equatorial bonds. With respect to this frame, the total and spin occupation of d_{z^2}, d_{xy}, d_{xz}, and d_{yz} is very close to one, indicating that they contain one majority (α) spin electron, and essentially no minority spin electrons. The $d_{x^2-y^2}$ occupation is, on the contrary, much smaller ($0.46|e|$), with contributions from both majority ($0.30|e|$) and minority ($0.16|e|$) spin electrons. We can sketch the situation in the octahedra as follows: the very low occupation of the $d_{x^2-y^2}$ orbital permits to shorten the equatorial bonds (which are about 0.4 Å shorter than the apical ones); the shorter bond favors, in turn, a back donation process from oxygen to the empty orbital, that involves mainly β electrons, because in this way the short range repulsion within the *d* shell is smaller. This picture is confirmed by the Mn-O bond population, which is non-negligible for the equatorial bonds ($0.027|e|$, whereas it is only $0.005|e|$ for the apical bonds), indicating some covalent character, and involves mostly β

TABLE II. Mulliken population data of electron charge ($\alpha+\beta$) and net spin ($\alpha-\beta$) for atomic orbitals in ferromagnetic Mn_3O_4. *s* and *l* superscripts indicate short (equatorial) and long (apical) Mn-O bonds, respectively.

	Mn_B		Mn_A		O	
	$\alpha+\beta$	$\alpha-\beta$	$\alpha+\beta$	$\alpha-\beta$	$\alpha+\beta$	$\alpha-\beta$
total *sp*	18.086	0.024	18.039	0.018	9.597	0.019
d_{xy}	1.025	0.952	1.009	0.976		
d_{xz}	1.025	0.974	1.028	0.974		
d_{yz}	1.027	0.973	1.028	0.974		
d_{z^2}	1.080	0.933	1.012	0.990		
$d_{x^2-y^2}$	0.465	0.139	1.026	0.990		
Total *d*	4.622	3.969	5.103	4.896	0.014	0.006
Net charge	+2.292		+1.858		−1.610	
B(Mn-O)	0.027^s	−0.020	−0.023	−0.037		
	0.005^l	−0.018				

electrons ($0.024|e|$, to be compared to $0.004\alpha|e|$). It must be noticed that, as the angles in the equatorial plane are not exactly equal to 90 degrees, the lobes of the *d* orbitals do not coincide with the equatorial bonds.

Additional information is provided by the total and projected density of states reported in Fig. 3 for the top valence and bottom conduction bands. As expected, the upper valence band is mainly contributed by *p*(O) states, whereas manganese *d* states (*s* valence states are empty) appear in the lower part of the valence band. *p*(O) states are spread over a large energy interval (about 0.2 Hartree) whereas Mn *d* states remain well localized. The Mn_B *d* states are lower in energy than the Mn_A ones; the energy difference is 3.2 eV; this value is to be compared to 1.4 eV, which is the difference between the two peaks attributed to Mn^{2+} and Mn^{3+} ions in high-resolution electron-energy-loss spectroscopy (HREELS) experiments.[31] This overestimation (of about a factor two) is in line with previous results for transition metal materials,[32] and is typical of the Hartree-Fock method. The t_{2g} and e_g derived states in Mn_B are at about the same energy. In the case of an ideal octahedron, d_{z^2} and $d_{x^2-y^2}$ should be at higher energy than d_{xy}, d_{xz}, and d_{yz}. In the present case, the lenghthening of the Mn_B-O bond parallel to the local *z* direction produces an energy lowering of the d_{z^2} orbital with respect to the $d_{x^2-y^2}$, down to the energy interval where the t_{2g} derived states present a maximum.

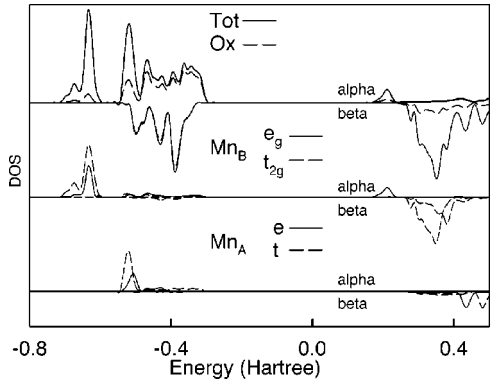

FIG. 3. Total and projected density of state of Mn_3O_4.

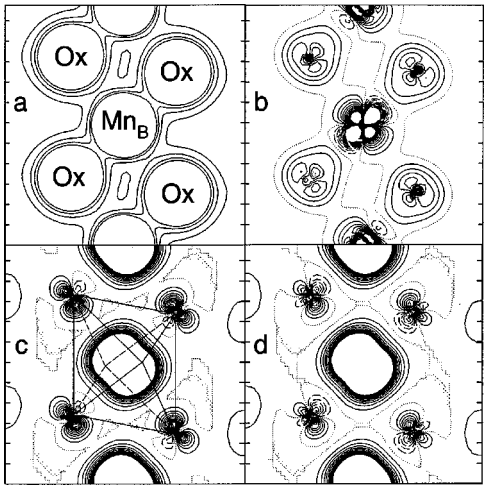

FIG. 4. Total (a), difference (b), and spin density (c,d) maps in a plane containing oxygen atoms 1,2,6,4 (Figs. 1 or 2) and manganese atom *B* (Fig. 2). Two equatorial and two apical Mn-O bonds are reported. Manganese at the top and bottom of figures are slighlty off plane. In (c) the octahedron is sketched. The difference map (b) is obtained by subtracting the superposition of spherical ionic charge densities (Mn_B^{3+} and O^{2-}) from the bulk charge density; the same bulk basis set has been used in the two cases. The spin density maps (c and d) refer to the FEM and FIM_4 solutions. The step between isodensity lines is 0.025, 0.01, and 0.005 e/Bohr^{-3} for the total, difference, and spin density maps, respectively. Dashed, dotted, and solid lines correspond to negative, zero, and positive values, respectively.

Total charge and difference density maps are shown in Fig. 4. The difference map shows that the density around oxygen is strongly deformed (with respect to the spherical shape) along the short Mn_B-O bond, whereas the effect is much smaller or negligeable along the long Mn_B-O bond. This supports the relative covalent character of the equatorial bond with respect to the apical ones, proposed previously. This may be traced back to Jahn-Teller distortion illustrated on Fig. 4(b) by a depletion of charge on Mn_B along the short Mn_B-O bond (in order to provide room to the protruding oxygen electrons, one could say) and a build up in the apical direction. The not shown electronic density around Mn_A remain very similar to the one of the isolated ion.

C. Ferromagnetic and ferrimagnetic states

Spinels are well known for their ferrimagnetism, mainly due to antiferromagnetic interactions between the *A*-*B* sublattices.[20] The *A*-*A* interactions are usually very small, because tetrahedra are not directly connected. *B*-*B* interactions are usually weaker than the *A*-*B* one's, but control the *B* sublattice magnetic configuration. In Mn_3O_4, apparently intra- and intersublattice interactions are comparable, and the collinear magnetic structure in *B* chains is destabilized.[17,18] Within the *B* sublattice, the spins adopt a canted Yafet-Kittel like structure.[17,18]

Comparison of the calculated and experimental spin distribution calls for some comments. Canted spin distribution can be understood at classical level in terms of lattice frustration. The assumed ideal (colinear) antiferromagnetic coupling is not consistent with the structure. At quantum level,

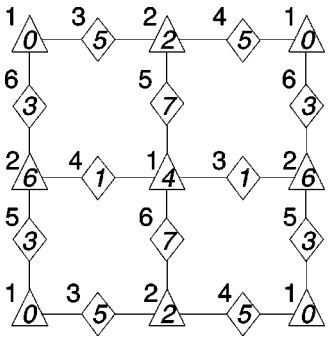

FIG. 5. Projected position of manganese on the ab plane of the conventional cell. Diamonds and triangles correspond to octahedral and tetrahedral manganese, respectively. Enclosed numbers indicate the altitude in eighths along the $\underline{c}$ axis, numbers outside symbols correspond to the numbering of manganese atoms.

spin-orbit coupling must be taken into account. Within the Hartree-Fock approximation, spin is an independent variable and spin-orbit coupling is not described. Then, comparison of the presently called ferrimagnetic states with the experimental magnetic structures is ambiguous. But, the relative intensity of the different first neighbor intercationic magnetic coupling can be estimated.

We have been able, however, to compute the total energy of a certain number of magnetic structures; from the energy differences between them, useful information on the strength and sign of the magnetic interactions can be extracted. Apart from the ferromagnetic (FEM) structure, six ferrimagnetic (FIM) configurations have been considered that do not require unit cells larger than the FEM one. If the manganese atoms of the primitive cell are labeled 1 to 6, the FEM solution will be indicated as: ($\uparrow$, $\uparrow$; $\uparrow$, $\uparrow$; $\uparrow$, $\uparrow$). Atoms 1 and 2 are at a tetrahedral site; 3 and 4 belong to a chain of octahedra (say along $\underline{a}$) and 5 and 6 to a chain perpendicular to it (along $\underline{b}$). Tetrahedral and octahedral manganese positions are shown projected in the ab plane of the conventional cell in Fig. 5. The following FIM configurations have also been taken into account: $\mathrm{FIM}_1=(\downarrow,\downarrow;\uparrow,\uparrow;\uparrow,\uparrow)$, $\mathrm{FIM}_2=(\uparrow,\downarrow;\uparrow,\uparrow;\uparrow,\uparrow)$, $\mathrm{FIM}_3=(\uparrow,\uparrow;\downarrow,\downarrow;\uparrow,\uparrow)$, $\mathrm{FIM}_4=(\uparrow,\uparrow;\uparrow,\downarrow;\uparrow,\downarrow)$, $\mathrm{FIM}_5=(\uparrow,\uparrow;\downarrow,\uparrow;\uparrow,\uparrow)$, and $\mathrm{FIM}_6=(\uparrow,\downarrow;\uparrow,\downarrow;\uparrow,\downarrow)$. They correspond to 6, 16, 10, 10, 18, and 0, uncoupled electrons per cell, respectively. All the calculations refer to the FEM optimized geometry; in order to limit the computational costs, the basis set without d orbitals on oxygen has been used.

The Hartree-Fock total energies for the seven configurations here considered are given in Table III. FIM states are always more stable than the FEM one, with the only exception of FIM_3, which is as stable as FEM. FIM_1, which is third in the stability scale, corresponds to antiferromagnetic interaction between octahedral and tetrahedral sublattices. The energy gain with respect to the FEM state indicates that antiferromagnetic intersublattice interactions are stabilizing and large, as expected. ΔE for FIM_2 is about half that for FIM_1, because only half of the FIM_1 interactions remain active. The interpretation of the results for the FIM_{3-6} states is somehow more difficult, and requires the analysis of the ferro- and antiferromagnetic *A-B* inter-sublattice and *B-B* intra sublattice interactions. We refer to Sec. II for a description of the Mn-Mn paths. We remind here that, as a general rule, the superexchange interaction decreases when the Mn-O distance increases, and when the Mn-O-Mn angle approaches to 90 degrees. FIM_6 is the most stable configuration, because spins alternate along both kind of octahedral chains as well as in the tetrahedral sublattice, in agreement with its status of closer configuration to the experimental one's. FIM_4 is very close in stability to FIM_6, as expected, because the only difference is in the tetrahedral sublattice (all spins up), and the *A-A* interaction is expected to be very small, as the tetrahedral sites are far apart from each other. In FIM_3 Mn atoms belonging to the same chain do have the same spin; in this configuration then only half of the *A-B* interactions remain active, together with the interchain interactions; as the formers are antiferromagnetic, and ΔE for FIM_3 is very close to zero, we must deduce that the latter is ferromagnetic.

TABLE III. Total energies E_{HF} per unit cell (in Hartree, and at the optimized FEM geometry) for the ferromagnetic (FEM) and the different ferrimagnetic (FIM) structures considered here. ΔE are the energy differences with respect to the ferromagnetic (FEM) solutions (all manganese spins up). δE is the same quantity evaluated by using the four superexchange coupling constants J_{AA}, J_{AB}, J_{BBs}, J_{BBl} (see text for more details).

Solution	E_{HF}	ΔE_{HF}	δE
FEM	−7498.51758	—	—
FIM_1	−7498.52001	−0.00243	−0.00230
FIM_2	−7498.51886	−0.00128	−0.00147
FIM_3	−7498.51776	−0.00018	−0.00016
FIM_4	−7498.52106	−0.00347	−0.00362
FIM_5	−7498.51906	−0.00148	−0.00156
FIM_6	−7498.52114	−0.00356	−0.00337

We can try to estimate in a more quantitative way the various magnetic interactions in our FIM structures by using a simple model spin Hamiltonian, such as the Ising one. In this model, under the hypothesis of the additivity of the spin-spin interactions, the energy difference ΔE between FIM's and FEM configurations can be written as:

$$\Delta E_{\mathrm{FIM-FEM}} = -2\sum_{ij} Z_{ij} S_i S_j J_{ij}$$

where S_i, S_j are the spins of cations i and j (we used 3.97/2 and 4.90/2 for the two kinds of Mn atoms, see Table II), J_{ij} is the superexchange coupling constant between them, and Z_{ij} is the number of i-j neighbors. The summation usually extends to first or second neighbors, as the J constants are known to fall down exponentially with distance, as already mentioned above. In the present case four superexchange constants have been considered, namely J_{AA}, J_{AB}, J_{BBs} (interaction within the $\underline{a}$ or $\underline{b}$ octahedral chains, short distance, cf. Fig. 1), and J_{BBl} (interchain interaction, long distance). Disregarding all the other interactions, and taking into account the number of neighbors for each kind of J, the above formula becomes, in the six cases here considered:

$$\Delta E_1 = 48 J_{AB} S_A S_B,$$

$$\Delta E_2 = 24 J_{AB} S_A S_B + 8 J_{AA} S_A^2,$$

TABLE IV. Experimental and calculated superexchange parameters.

	calc. (K)	exp.[19] (K)	Error (%)
J_{AA}	−42.13	−4.9	57
J_{AB}	−3.11	−6.8	54
J_{BBl}	+4.95		
J_{BBs}	−29.7		
$J_{BB}(mean)$	−6.57	−19.9	67

$$\Delta E_3 = 24J_{AB}S_AS_B + 16J_{BBl}S_B^2,$$

$$\Delta E_4 = 24J_{AB}S_AS_B + (8J_{BBl} + 8J_{BBs})S_B^2,$$

$$\Delta E_5 = 12J_{AB}S_AS_B + (8J_{BBl} + 4J_{BBs})S_B^2,$$

$$\Delta E_6 = 8J_{AA}S_A^2 + 12J_{AB}S_AS_B + (8J_{BBl} + 8J_{BBs})S_B^2,$$

where the ΔE values are given in Table III. The J values obtained by best fit from these data are quoted in Table IV. The strongest interaction is the *B*-*B* one within the $\underline{a}$ or $\underline{b}$ chains; the *A*-*A* and *A*-*B* ones are about ten times smaller; the *B*-*B* interchain coupling favors the ferromagnetic arrangements. If the obtained J values are inserted in the six equations, the δE values reported in the third column of Table III are obtained; the quite good agreement between the ΔE and δE values indicates that the model includes all the most relevant magnetic interactions, and that the overall accuracy of the calculation is very high; we underline in fact that the J constants are as small as a microhartree.

The calculated J parameters are about 40−50% of those derived from experimental data,[19] as shown in Table IV. It must be noticed that in Ref. 19 a single J_{BB} constant is provided, corresponding to the weighted mean value between J_{BBs} and J_{BBl}, whereas we have been able to estimate the two interactions separately. The percentage error (see third column of Table IV) is about the same as that obtained for other compounds such as the KMF_3[11,12] perovskite, and K_2MF_4[10] layered perovskite, and is mainly due to the fact that the UHF method disregards the interelectronic correlation. These data confirm that the performances of the method remain good also when systems with large unit cells and complicated spin-spin interactions are considered.

Calculated exchange parameters clearly indicate a strong antiferromagnetic interaction within $\underline{a}$ and $\underline{b}$ chains and a weaker ferromagnetic ordering between $\underline{a}$ and $\underline{b}$ chains. The interchain connectivity as shown in Fig. 2 is not fully compatible with colinear interactions. Lattice frustration is expected. Its consequence on spin distribution have not been investigated for the moment, but should induce deparallelisation of the atomic spins.

The Curie temperature calculated with the formula proposed in Refs. 19,33 is 34 K. It underestimates by 20% the experimental one of 42 K.[17–19,34,35]

Spin ($\alpha-\beta$) density maps are very useful for the interpretation of the superexchange mechanism. The spin density of FEM and FIM_4 in three different planes is shown in Fig. 4 and Fig. 6. The different occupation of the d shell in Mn_A and Mn_B is very evident from the three figures: Mn_A, that has essentially a d^5 occupation, is nearly spherical [Fig. 6(a)], with a small deformation due to the electrostatic influence of the neighboring oxygen atoms. In Mn_B, only four d orbitals are occupied; in the local octahedral frame $d_{x^2-y^2}$ is empty, as is clearly shown by Fig. 6(c),(d), and the ion takes the cylinderlike structure shown by Fig. 4(c),(d) and Fig. 6(a),(b). Most of the spin density is on the Mn atoms (about five and four electrons, see Table II); the most interesting part of the maps, however, is the very small spin polarization of the oxygen ions (the integrated spin density on oxygen is about $0.02|e|$), because it is through this polarization that the magnetic interaction between two manganese atoms takes place. It is useful to underline that the relative stability between different spin phases is very small (of the order of a millihartree), and that it is determined by a quite small spin polarization of the bridging anions. The oxygen ion in our case is then surrounded by four Mn ions (see Fig. 1); as the valence *sp* shell on Mn is empty, the most external shell of Mn, which is the one that is in contact with the oxygen ion, is the d shell, which contains four or five electrons with the same spin. In the case of the FEM structure, for example, each oxygen atom is surrounded by four Mn ions with α spin; in order to reduce the short range Pauli repulsion, the oxygen ion will try to displace his α electrons (β electrons will simply feel the electrostatic repulsion from the Mn electrons) from the contact zone. This behavior is evident in Fig. 6(a), where spin density peaks appear protruding away from the Mn atoms. There is no polarization in Fig. 6(c), because it contains four equatorial (short) Mn-O bonds; Fig. 4 shows that polarization effect can take place along the long Mn-O bond, as the Pauli repulsion is very short range; the oxygen ion is then depleting the p orbital along the short Mn-O bond, and building up spin density in the direction orthogonal to it. The FIM picture in the two figures show that in this structure the oxygen ion has additional freedom for trying to reduce the Pauli repulsion: α electrons are displaced towards the Mn ions with β d shell, and vice versa, as can be appreciated by looking carefully at the positive (continuous lines)

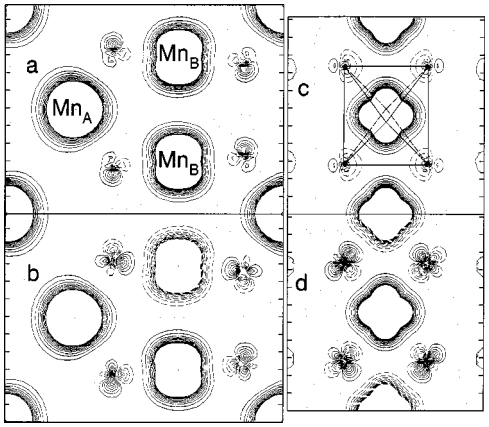

FIG. 6. Spin density maps of the octahedron for FEM configuration (a) and (c), and FIM_4 one's (b) and (d). Planes (a),(b) contain atoms labeled b, c, and e in Fig. 2. Oxygen is slightly off plane (0.22 Å). Planes (c),(d) contain oxygen atoms labeled 2, 3, 4, and 5 (Figs. 1 and 2) and manganese atom *B* (Fig. 1). Manganese at the top and bottom of figure are slightly off plane. Mn_B-O bonds are all equatorial. Shape of the octahedron is reported on plane c. Scale symbols and other details as in Fig. 4.

and negative (dashed lines) lobes of the oxygen spin density shown in the two figures. The different behavior is particularly evident in Figs. 4 and 6.

V. CONCLUSION

The present study has shown that *ab initio* methods can be applied, in conjunction with an *all electron* basis set, to the study of the structural, electronic and magnetic properties of a relatively complicated compound such as Mn_3O_4. In particular, an homogeneous and coherent description has been reached of the electronic situation at the two Mn sites, manely the tetrahedral one, where the ion is nearly spherical and can be described as d^5 Mn^{2+}, and the octahedral one, where the ion is in a d^4 configuration, is Jahn-Teller distorted (with two quite different bond distances in the equatorial plane and in the direction orthogonal to it) and shows an interaction with the oxygen atoms that is certainly not as ionic as for the tetrahedral Mn atom. As regards the magnetic interactions, which are very difficult to describe as they involve quite small energy differences, a certain number of interesting results has been obtained: (i) six FIM (ferrimagnetic) structures have been considered, and all of them are more stable than the FEM (ferromagnetic) one; (ii) the most important magnetic interaction is the Mn_B-Mn_B one, which involves Mn atoms of the same octahedral chain running along $\underline{a}$ or $\underline{b}$; the interaction between Mn_B atoms belonging to different chains is ferromagnetic, and of the same order of magnitude as the Mn_A-Mn_B, which is antiferromagnetic; (iii) the calculated superexchange coupling constants J are in semiquantitative agreement with those obtained from experimental data, when available.

[1] R. Dovesi, V.R. Saunders, C. Roetti, M. Causà, N.M. Harrison, R. Orlando, and E. Aprà, *CRYSTAL95 User's Manual*, (University of Torino, Torino, 1996).

[2] W. C. Mackrodt, N. M. Harrison, V. R. Saunders, N. L. Allan, M. D. Towler, E. Aprà, and R. Dovesi, Philos. Mag. A **68**, 653 (1993).

[3] W. Mackrodt and E. Williamson, J. Phys.: Condens. Matter **9**, 6591 (1997).

[4] M. D. Towler, N. L. Allan, N. M. Harrison, V. R. Saunders, W. C. Mackrodt, and E. Aprà, Phys. Rev. B **50**, 5041 (1994).

[5] M. Catti, G. Valerio, and R. Dovesi, Phys. Rev. B **51**, 7441 (1995).

[6] M. Catti, G. Sandrone, G. Valerio, and R. Dovesi, J. Phys. Chem. Solids **57**, 1735 (1996).

[7] M. Catti, G. Sandrone, and R. Dovesi, Phys. Rev. B **54**, 16122 (1997).

[8] M. Catti and G. Sandrone, Faraday Discuss. **106**, 189 (1997).

[9] J. M. Ricart, R. Dovesi, C. Roetti, and V. R. Saunders, Phys. Rev. B **52**, 2381 (1995).

[10] R. Dovesi, J. M. Ricart, V. R. Saunders, and R. Orlando, J. Phys.: Condens. Matter **7**, 7997 (1995).

[11] M. D. Towler, R. Dovesi, and V. R. Saunders, Phys. Rev. B **52**, 10150 (1995).

[12] R. Dovesi, F. Freyria Fava, C. Roetti, and V. R. Saunders, Faraday Discuss. **106**, 173 (1998).

[13] R. D. G. Valerio, M. Catti, and R. Orlando, Phys. Rev. B **52**, 2422 (1995).

[14] I. de P.R. Moreira, R. Dovesi, C. Roetti, V.R. Saunders, and R. Orlando, Phys. Rev. B (to be published).

[15] L. J. De Jongh, Physica B & C **79B**, 568 (1975).

[16] J. S. Kasper, Bull. Am. Phys. Soc. **4**, 178 (1959).

[17] B. Boucher, R. Buhl, and M. Perrin, J. Phys. Chem. Solids **32**, 2429 (1971).

[18] G. Jensen and O. Nielsen, J. Phys. C **7**, 409 (1974).

[19] G. Srinivasan and M. S. Seehra, Phys. Rev. B **28**, 1 (1983).

[20] S. Kupricka and P. Novak, *Ferromagnetic Materials* (North-Holland, Amsterdam, 1982).

[21] E. Paris, C. R. Ross, and H. Olijnyk, Eur. J. Mineral. **4**, 87 (1992).

[22] C. R. Ross, D. C. Rubie, and E. Paris, Am. Mineral. **75**, 1249 (1990).

[23] C. Pisani, R. Dovesi, and C. Roetti, *Hartree Fock ab initio Treatment of Crystalline Systems*, Lecture Notes in Chemistry (Springer-Verlag, Heidelberg, 1988), Vol. 48, pp. 193.

[24] F. Freyra Fava, I. Bataille, A. Lichanot, C. Larrieu, and R. Dovesi, J. Phys.: Condens. Matter **9**, 10 715 (1997).

[25] K. Satomi, J. Phys. Soc. Jpn. **16**, 258 (1960).

[26] D. Jarosch, Contrib. Mineral. Petrol. **37**, 15 (1987).

[27] P. D'Arco, B. Silvi, C. Roetti, and R. Orlando, J. Geophys. Res. **96**, 6107 (1991).

[28] R. Dovesi, C. Roetti, C. Freyra Fava, E. Aprà, V.R. Saunders, and N.M. Harrison, Philos. Trans. R. Soc. London, Ser. A **341**, 203 (1992).

[29] R. A. Robie, B. S. Hemingway, and J. R. Fisher, *Thermodynamic Properties of Minerals and Related Substances at 298.15 K and 1 Bar* (10^5 *Pascals) Pressure and at Higher Temperatures*, U. S. Geol. Surv. Bull. No. 1452 (U.S. GPO, Washington, D.C., 1979).

[30] R. Dovesi, *Quantum-Mechanical Ab-initio Calculation of the Properties of Crystalline Materials*, Lect. Notes Chem., edited by C. Pisani (Springer-Verlag, Berlin, 1996), Vol. 67, pp. 179–208.

[31] L. Garvie and A. Craven, Phys. Chem. Miner. **21**, 191 (1994).

[32] W. C. Mackrodt, N. M. Harrison, V. R. Saunders, N. L. Allan, and M. D. Towler, Chem. Phys. Lett. **250**, 66 (1996).

[33] F. K. Lotgering, Philips Res. Rep. **11**, 190 (1956).

[34] O. V. Nielsen, J. Phys. (France) **32-C1**, 51 (1971).

[35] O. V. Nielsen and L. W. Roeland, J. Phys. C **9**, 1307 (1976).